RSC Advances

PAPER

View Article Online
View Journal | View Issue

Cite this: *RSC Adv.*, 2025, **15**, 27452

Porous titania-coated zirconia: preparation and osteogenic performance evaluation

Shuang Tang, [a] Yaoxin Wang,[a] Ping Ma[a] and Zhipeng Fan*[b]

Zirconia implants are increasingly prevalent in dental applications due to their superior aesthetic outcomes, excellent mechanical properties, and remarkable biocompatibility. However, zirconia implants face challenges such as insufficient bioactivity and limited osseointegration capability, which compromise their long-term stability. In this study, porous titania (TiO_2) coatings were developed on zirconia surfaces to enhance their osteogenic activity. Zirconia substrates were immersed in a mixed solution of zirconium oxychloride ($ZrOCl_2$) and TiO_2 in a water bath. By regulating the concentration of the treatment solution according to the hydrolysis characteristics of $ZrOCl_2$, TiO_2 coatings with different porous morphologies were formed during the dense sintering process of zirconia ceramics. The surface characteristics, mechanical strength and bonding strength of coatings of different zirconia samples were tested. The MC3T3-E1 cells were seeded on zirconia discs to evaluate the bioactivity of porous TiO_2 coatings. To assess the *in vivo* response of porous TiO_2-coated zirconia, the samples were implanted into rat femurs, followed by systematic analysis. Firmly bonded porous TiO_2 coatings were generated on the zirconia surface, significantly enhancing surface roughness and hydrophilicity without adversely affecting the mechanical strength of zirconia. Through *in vitro* cell experiments, porous TiO_2-modified zirconia could promote cell proliferation, spreading and osteogenic differentiation. Furthermore, *in vivo* assessments confirmed that porous TiO_2-coated zirconia exhibited superior osseointegration effect. The preparation of porous TiO_2-coated zirconia is an effective method to improve the osteogenic performance of zirconia implants, which is of significant importance for promoting the widespread application of zirconia implants.

Received 20th May 2025
Accepted 29th July 2025

DOI: 10.1039/d5ra03550c

rsc.li/rsc-advances

1. Introduction

Tooth loss and dentition defects can significantly impact patients' physiological and psychological health. Dental implant restoration can restore patients' masticatory function, thereby improving their quality of life.[1,2] Zirconia has emerged as a substitute material for titanium and titanium alloy implants due to its excellent mechanical properties and aesthetic characteristics.[3,4] Zirconia exhibits a flexural strength exceeding 1000 MPa, a fracture toughness of approximately 9 MPa $m^{1/2}$, and a compressive strength of about 2000 MPa.[5] These mechanical strengths create a foundation for its application as an implant material. Additionally, zirconia exhibits aesthetic effects similar to natural teeth and possesses excellent biocompatibility, which further enhances its advantages as an implant material.[6,7] While, zirconia is a bioinert material, which results in slower osseointegration and increases the failure rate of implant surgery.[8,9]

Surface modification treatments are applied to improve the osteogenic effects of the zirconia implant, including mechanical processing, sandblasting and acid etching.[10–12] These methods can increase the surface roughness of zirconia implants, thereby facilitating osseointegration. However, studies have found that such treatments may compromise its mechanical strength.[13] Moreover, to improve the osteogenic performance of zirconia, researchers have developed coatings with various components on its surface, such as β-tricalcium phosphate (β-TCP), hydroxyapatite (HA), and so on. Stefanic *et al.* reported the formation of a stable β-tricalcium phosphate (β-TCP) coating on zirconia implants *via* chemical deposition and hydrothermal treatment.[14] However, the bonding strength between the β-TCP coating and the zirconia substrate was relatively weak, particularly for coatings obtained through physical deposition methods. Miao *et al.* fabricated a porous layer on a zirconia substrate and deposited an HA coating to enhance the osteogenic properties of zirconia.[15] While, the mismatch in thermal expansion coefficients between HA and the zirconia substrate limited the bonding strength of the HA coating. In summary, surface modification process often faces

[a]*Beijing Institute of Dental Research, Beijing Stomatological Hospital, School of Stomatology, Capital Medical University, Beijing, China*

[b]*Laboratory of Molecular Signaling and Stem Cells Therapy, Beijing Key Laboratory of Tooth Regeneration and Function Reconstruction, Beijing Stomatological Hospital, School of Stomatology, Capital Medical University, Beijing, China. E-mail: zpfan@ccmu.edu.cn*

challenges due to poor interfacial bonding between the coating and the substrate.

The high polarity of Ti–O bonds in TiO_2 promotes the dissociation of surface water molecules into hydroxyl groups, thereby enhancing its bioactivity.[16] Miranda *et al.* successfully prepared a titania coating on zirconia *via* the sol–gel method, achieving excellent bioactivity.[17] Additionally, previous studies fabricated a titania coating on zirconia *via* plasma spraying and demonstrated that the TiO_2 coating significantly enhanced osteoblast differentiation *in vitro*.[18] However, the TiO_2 coatings obtained by these methods exhibited poor adhesion to zirconia, forming discontinuous and uneven layers. This could increase the risk of coating delamination at the bone-implant interface, compromising the long-term stability of zirconia implants. Therefore, a more effective approach is needed to produce strongly bonded TiO_2 coatings on zirconia surfaces. In our previous research, we developed an improved method for preparing titania coatings. In this method, pre-sintered zirconia was treated in a mixed suspension containing $ZrOCl_2$ and different concentrations of TiO_2, followed by dense sintering. As a result, TiO_2 coatings with varying distribution densities were obtained. The hydrolysis properties of $ZrOCl_2$ facilitate the formation of a Ti–Zr mixed interfacial layer, thereby ensuring strong bonding between the coating and the zirconia substrate. Furthermore, our previous work demonstrated that TiO_2 coatings with enhanced bioactivity, surface roughness, and wettability could be fabricated on pre-sintered zirconia using this strategy, thereby promoting osteogenic differentiation and osseointegration.[19] However, these coatings exhibited a relatively uniform, non-porous morphology, which limited available sites for cell adhesion, migration, and proliferation.

Studies have shown that porous surfaces facilitate cell adhesion and proliferation, extracellular matrix deposition, nutrient/oxygen transport, and metabolic waste removal, thereby providing structural conditions for bone tissue ingrowth.[20] The existing preparation techniques for porous zirconia ceramics primarily rely on the addition of pore-forming agents.[21] By removing these agents through sublimation, chemical leaching, or sintering, porous ceramics with irregular pores can be formed. However, this method may alter the internal structure of zirconia, potentially compromising its flexural strength.[22] In this study, we aim to reliably fabricate a porous titania coating on zirconia surfaces by controlling the dehydration of bound water in $ZrOCl_2$ hydrolysis products. Through optimizing the surface structure, the bioactivity of the coating can be further enhanced, thereby significantly improving the adhesion, proliferation, and differentiation of osteoblasts, ultimately promoting the osseointegration of zirconia implants. This treatment offers a novel strategy for fabricating porous coatings with strong substrate bonding, thereby broadening the potential biomedical applications of porous TiO_2-coated zirconia.

2. Materials and methods

2.1. Preparation of the samples

The pre-sintered zirconia ceramic blocks (Upcera, China) were processed into discs with a diameter of 14 mm and a thickness of 2 mm by a low-speed cutting machine (Buehler, USA). The zirconia discs were successively polished by 800#, 1000#, and 1200# SiC sandpaper, followed by ultrasonic cleaning with distilled water and anhydrous ethanol. All samples were randomly assigned into four groups. The control group (C) required no additional treatment. According to the concentration of $ZrOCl_2$ (as shown in Table 1), the experimental samples were divided into three groups: TO_1, TO_2 and TO_3. $ZrOCl_2$ was dissolved in deionized water at the predetermined concentration. Subsequently, a certain amount of nano TiO_2 powder (particle size: 20–30 nm, purity: 99%) was added into the $ZrOCl_2$ solution. The mixture was subjected to magnetic stirring and ultrasonic dispersion to ensure the TiO_2 powder was uniformly dispersed, resulting in a homogeneous suspension. The pre-sintered zirconia samples were then immersed in the suspension and reacted in a water bath at 95 °C for 4 h. After the water bath treatment, the samples were removed and gently rinsed several times with deionized water to remove any residual acids or impurities on the surface. After cleaning and drying, all samples were sintered in a sintering furnace (Everest, Kavo, Germany), heated to 1450 °C at a rate of 5 °C min^{-1} according to the instructions. Before use, all specimens were rinsed with deionized water and dried for storage.

2.2. Surface characterization of the samples

The surface and cross-sectional morphologies of each group of samples were observed using a scanning electron microscope (SEM, Phenom-world, Netherlands). Additionally, three-dimensional (3-D) reconstruction images of the surface of different zirconia discs were also captured by SEM. The porosity of the porous coatings was calculated using ImageJ software. The surface elemental mapping and cross-sectional line scanning were performed with an energy-dispersive X-ray spectrometer (EDS, Phenom-world, Netherlands). The X-ray diffraction (XRD, Shimadzu, Japan) analysis was conducted to identify the structures and phase compositions of the zirconia surfaces from each group. The water contact angle (WCA) was measured using an automatic contact angle meter (Kino Industry, USA) to evaluate surface hydrophilicity. For the measurements, 3 μL droplets of deionized water were deposited onto the surfaces of the testing discs. The average values obtained from the measurements ($n = 5$) were recorded and subsequently compared. The average surface roughness (R_a) of each group ($n = 5$) was measured using a surface roughness tester (Shanghai Taiming Optical Instrument, China).

2.3. Three-point bending strength testing

Pre-sintered zirconia ceramic blocks were prepared into strips (25 × 5 × 1.5 mm). Each group of samples ($n = 5$) was treated

Table 1 Concentration of treatment solution for experimental group specimens, mol L^{-1}

	$ZrOCl_2$	TiO_2
TO_1	1	1
TO_2	1.5	1
TO_3	2	1

according to the procedure described in Section 2.1. The flexural strength (σ) was evaluated by a universal material testing machine (Shimadzu, Japan) with a crosshead movement speed of 0.5 mm min^{-1}. The three-point bending strength of each specimen was calculated according to the formula: $\sigma = 3F_{l/2}wb^2$. Where F represents the breaking load (N), l is the test span (mm), w denotes the width of the sample (mm), and b is the thickness of the sample (mm).

2.4. The bonding strength of coating

The adhesion strength of the coating was tested using a tensile pull-off test with epoxy resin bonding. A universal material testing machine (AG-X Plus, Shimadzu, Japan) was employed to perform a pull-off test to obtain the adhesion strength of the TiO_2-coated zirconia specimens ($n = 5$). The bottom of the sample was fixed on the experimental machine platform. A transparent tape with a circular hole (4 mm in diameter) was applied to the coating surface to demarcate the bonding area. A resin column (4 mm in diameter and 5 mm in height) was then bonded to the coating using an adhesive (Kuraray Company, Japan). The coating was stretched at a speed of 0.5 mm min^{-1} until fracture occurred. The interfacial adhesion strength was calculated as follows:

$$P = F_{max}/S.$$

where P represents the bonding strength, F_{max} denotes the maximum load at fracture, and S signifies the bonding area.

2.5. *In vitro* cell experiments to assess the bioactivity of porous TiO_2-coated zirconia

2.5.1. Cell culture. Mouse pre-osteoblasts cells (MC3T3-E1) were purchased from the American Type Culture Collection to evaluate the biological response to different zirconia samples. The cells were maintained in α-MEM medium (Gibco, USA) supplemented with 10% fetal bovine serum (FBS, Gibco, USA) and 1% penicillin-streptomycin (Gibco, USA) at 37 °C in a humidified environment with 5% CO_2.

2.5.2. Live/dead double staining. Zirconia specimens ($n = 3$) were placed in a 24-well plate, with a seeding density of 1×10^4 cells per well for MC3T3-E1 cells. The cells were cultured at 37 °C in a 5% CO_2 incubator for 1 and 3 days. The staining solution was prepared by mixing 6 μL of calcein-AM and 18 μL of propidium iodide in 6 mL of 10× assay buffer. After thorough mixing, 200 μL staining solution was added to each well. After 30 min of staining, the samples were observed under fluorescence microscope (Olympus, Japan).

2.5.3. CCK-8 assay. MC3T3-E1 cells were seeded on the surface of each group of specimens ($n = 3$) at a density of 2.5×10^4 cells per mL. After culturing for 1, 3, and 5 days, 400 μL α-MEM containing 40 μL CCK-8 solution (Dojindo, Japan) was added to each well, and the samples were incubated at 37 °C for 1 h. After incubation, 200 μL of the supernatant from each well was transferred to a fresh 96-well plate. The 96-well plate was placed in a microplate reader to measure the absorbance. The absorbance was measured with a microplate reader (Molecular Devices, USA) at 450 nm.

2.5.4. Cytoskeleton immunofluorescence staining. MC3T3-E1 cells were seeded on zirconia samples ($n = 3$) in a 24-well plate at a density of 1×10^4 cells per well. After being cultured for 1 and 3 days, the cells on different specimens were fixed with 4% paraformaldehyde and permeabilized with 0.1% Triton X-100. Finally, MC3T3-E1 cells were stained with phalloidin (Sigma, USA) and 10 μg per mL DAPI (Sigma, USA) respectively, followed by three thorough washes with PBS. The stained MC3T3-E1 cells were observed by a fluorescence microscope (Olympus, Japan).

2.5.5. Staining and quantification of ALP activity. The zirconia specimens from each group ($n = 3$) were placed in a 24-well plate, and MC3T3-E1 cells at a density of 2.5×10^4 cells per mL were co-cultured for 24 h. After removing the existing medium, osteogenic medium mixed with 50 μg per mL L-ascorbic acid (Sigma, USA), 10 mM β-glycerol phosphate (Sigma, USA) and 50 nM dexamethasone (Sigma, USA) was added. After culturing in osteogenic induction medium for 4 and 7 days, the samples were fixed in 4% paraformaldehyde and stained with a BCIP/NBT Kit (Beyotime, China). The staining results were observed by stereomicroscopy (Olympus, Japan). The ALP activity was quantified following the protocol provided with the detection kit (Beyotime, China). The results were standardized to the total protein concentration, which was measured by a BCA protein assay kit (Beyotime Biotechnology, China).

2.5.6. Alizarin red S staining and quantitative analysis. Each group of samples ($n = 3$) were placed in a 24-well plate, and 1 mL of cell suspension (1×10^5 cells per mL) was added. After incubating for 24 h, the osteogenic induction medium was replaced. After 7 days of osteogenic induction, the samples were stained with 0.2% Alizarin Red solution (pH 4.2, Sigma, USA) and observed by a stereomicroscope (Olympus, Japan). For quantitative analysis, 10% cetylpyridinium chloride (Sigma, USA) was added to dissolve stained mineralized nodules on the surface of the samples. The OD value was measured at 600 nm by microplate reader (Molecular Devices, USA).

2.5.7. qRT-PCR analysis. MC3T3-E1 cells were seeded on the surfaces of each group of specimens ($n = 3$) at a density of 1×10^5 cells per well. After 7 days of osteogenic induction, the quantitative reverse transcription-polymerase chain reaction (qRT-PCR) was employed to evaluate the expression levels of osteogenic genes including ALP, type I collagen (Col-I), osteocalcin (OCN), runt-related transcription factor 2 (Runx2) and osteopontin (OPN). Total RNA was extracted using the TRIzol reagent (Sigma, USA). The RNA was reverse transcribed into cDNA by the Reverse Transcription Takara kit (Takara, Japan). Finally, quantitative RT-PCR was performed using SYBR Green chemistry (Takara, Japan). Primers for osteogenesis-related genes are listed in Table 2. Relative mRNA expression levels were calculated using the $2^{-\Delta\Delta C_t}$ method with GAPDH as the housekeeping gene.

2.6. *In vivo* animal experiments

2.6.1. Specimen preparation. The pre-sintered zirconia cylinders (diameter 1 mm, length 10 mm) was randomly divided

Table 2 Primers for target genes

Target genes	Primers
ALP	F: 5′-TGCCCTGAAACTCCAAAAGC-3′
	R: 5′-CTTCACGCCACACAAGTAGG-3′
COl-I	F: 5′-CTGACTGGAAGAGCGGAGAG-3′
	R: 5′-GACGGCTGAGTAGGGAACAC-3′
OCN	F: 5′-AGACTCCGGCGCTACCTT-3′
	R: 5′-CTCGTCACAAGCAGGGTTAAG-3′
Runx2	F: 5′-AGATGGGACTGTGGTTACCG-3′
	R: 5′-TAGCTCTGTGGTAAGTGGCC-3′
OPN	F: 5′-ACACTTTCACTCCAATCGTCCCTAC-3′
	R: 5′-GGACTCCTTAGACTCACCGCTCTT-3′
GAPDH	F: 5′-ATGGGTGTGAACCACGAGA-3′
	R: 5′-CAGGGATGATGTTCTGGGCA-3′

into 4 groups: group C served as the control group. The experimental group samples were immersed in different concentrations of $ZrOCl_2$ solution mixed with TiO_2 (as shown in Table 1), named as TO_1, TO_2 and TO_3 groups. After sintering, each group of specimens were disinfected at 121 °C for 15 min before being used in subsequent experiments.

2.6.2. Surgical procedure. All *in vivo* experiments were approved by the ethics committee of Beijing Stomatological Hospital affiliated with Capital Medical University and in accordance with the "Guide for the Care and Use of Laboratory Animals". Eight-week-old male Sprague Dawley (SD) rats ($n = 3$) were randomly divided into four groups: C, TO_1, TO_2 and TO_3. The rats were anesthetized by intraperitoneal injection of sodium pentobarbital. Subsequently, the hind limbs of each rat were shaved and sterilized. A 10 mm incision was made on the medial side of the knee joint, followed by blunt dissection of the muscles, patella, and associated ligaments to fully expose the femur. A bone defect of 1 mm in diameter and 10 mm in length was prepared and cooled with saline to prevent osteonecrosis. The implants were carefully and gently inserted into the prepared cavities, after which the surrounding soft tissues were meticulously sutured to ensure proper closure. To prevent the risk of postoperative infection, penicillin (100 000 IU) was administered *via* intramuscular injection. After 4 and 8 weeks of implantation, the rats were sacrificed. The femurs, along with the implants, were collected and fixed in 4% paraformaldehyde before conducting further assessments.

2.6.3. Micro-CT analysis. High-resolution micro-CT (Skyscan, Bruker) was employed to scan the femurs. Three-dimensional reconstruction was performed using CTvox software, and the images were analyzed and processed with CTAn software. After image binarization and 3D denoising, a circular region of interest (ROI) with a diameter of 1.5 mm was selected to cover the bone defect area. The main bone-related parameters: bone-to-tissue volume ratio (BV/TV), trabecular thickness (Tb. Th), trabecular separation (Tb. Sp), and trabecular number (Tb. N) were calculated and compared.

2.6.4. Histological analysis. Bone tissue samples containing implants from each group were placed in a 10% ethylenediaminetetraacetic acid (EDTA) solution for decalcification. Once decalcification was complete, the implants were carefully removed to ensure that the surrounding new bone was not damaged. The decalcified samples underwent a series of processing steps, including ethanol gradient dehydration, xylene clearing, paraffin embedding, and sectioning. Finally, hematoxylin and eosin (H&E) staining and Masson staining were performed. These sections were observed by microscopy (Olympus, Japan).

2.7. Statistical analysis

All quantitative data were expressed as mean ± standard deviation (SD). The differences between the groups were assessed by one-way analysis of variance (ANOVA) with least significant difference (LSD) post hoc tests in IBM SPSS Statistics (Version 22.0, Windows). A p-value < 0.05 was considered statistically significant.

3. Results and discussion

3.1. Surface characterization

Porous titania coatings with different morphologies were successfully prepared on the zirconia surface (as shown in Fig. 1A–C). With increasing $ZrOCl_2$ concentration in the treatment solution (TO_1 < TO_2 < TO_3), the surface porosity rose sequentially to 18.36 ± 0.96% (TO_2) and 43.08 ± 1.08% (TO_3), as quantified by ImageJ analysis. SEM observation of the longitudinal sections of each group of samples (Fig. 1D) revealed that the titania coatings formed on the surfaces of the TO_1, TO_2, and TO_3 group specimens were tightly bonded to the zirconia substrate, with no obvious cracks. The TO_3 group exhibited a higher density of interconnected pores compared to the TO_2 group.

Based on the hydrolysis characteristics of $ZrOCl_2$: $ZrOCl_2 + 2H_2O \rightarrow ZrO(OH)_2 + 2HCl$; $ZrO(OH)_2 + H_2O \rightarrow Zr(OH)_4$; $Zr(OH)_4 \rightarrow ZrO_2 + 2H_2O$. Increasing $ZrOCl_2$ concentration accelerates $Zr(OH)_4$ formation, and its subsequent dehydration during sintering generates higher porosity in the TiO_2 coating.

The surface elemental mapping results are shown in Fig. 2A. The control group exhibited Zr, O, and Y as the primary elements on the zirconia surface. The TO_1, TO_2 and TO_3 groups mainly consisted of Ti and O, along with trace amounts of Zr. As illustrated in Fig. 2B, line scanning was performed to analyze the elemental composition variation across the longitudinal sections of each group. The trend of elemental changes along the cross-section of the specimens revealed the formation of a Ti–Zr mixed layer at the surface of the zirconia substrate.

The fabrication strategy in this study effectively leveraged the high porosity of pre-sintered zirconia to facilitate $ZrOCl_2$ infiltration. Upon hydrolysis, $ZrOCl_2$ transformed into $Zr(OH)_4$, which decomposed into ZrO_2 during sintering, enhancing interfacial bonding. Concurrently, TiO_2 diffused into the zirconia substrate, forming a chemically stable Ti–Zr mixed interface. This explains the gradual transition in elemental composition observed in line scanning (Fig. 2B), where Ti intensity decreased while Zr increased toward the substrate.

Fig. 3A shows the XRD results, indicating that group C zirconia exhibited a tetragonal structure. The crystal structure

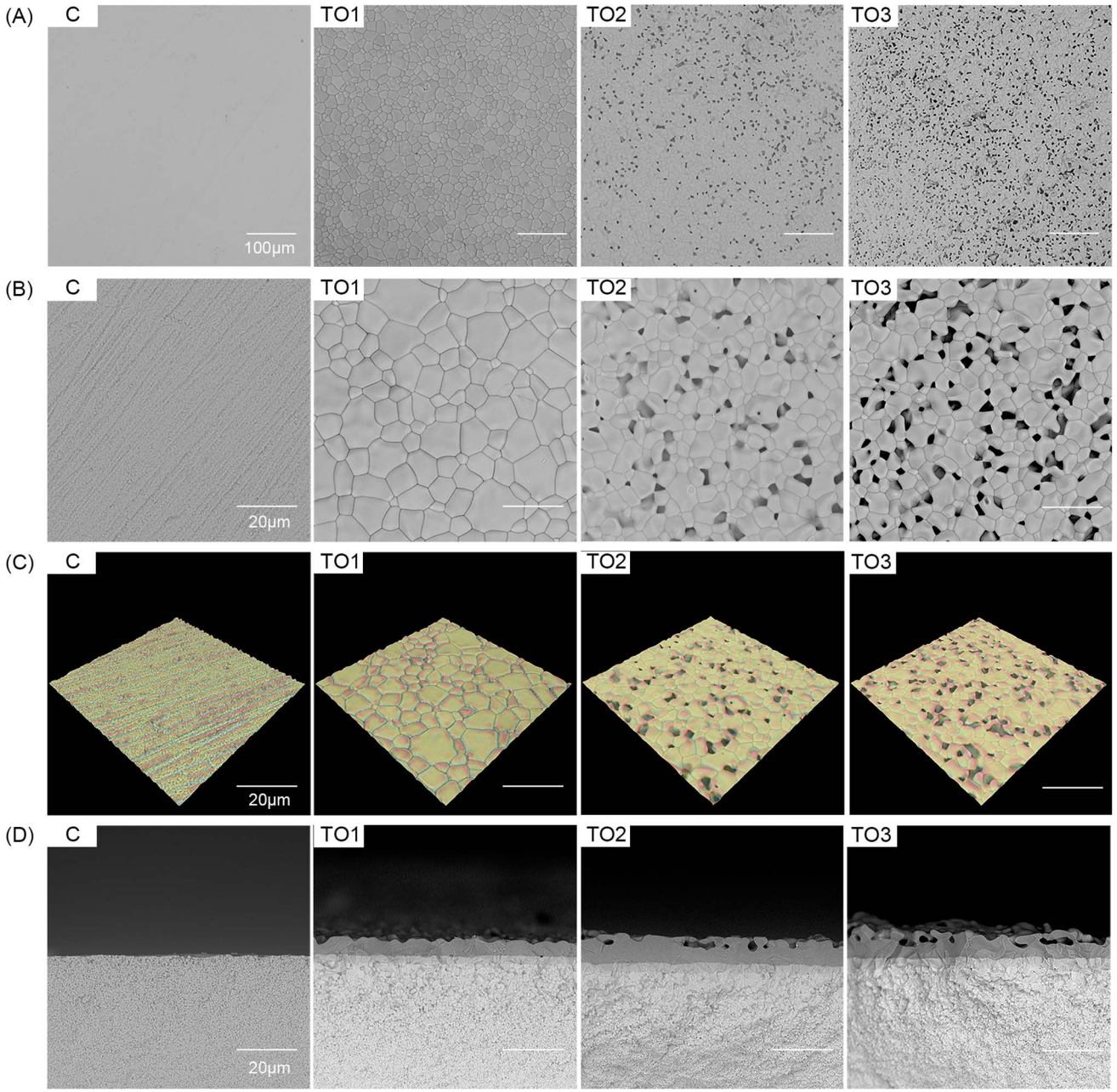

Fig. 1 SEM images of the samples: (A) low magnification (scale bar: 100 μm), (B) high magnification (scale bar: 20 μm). (C) 3-D reconstruction images of zirconia specimens in each group. (D) Cross-sectional SEM images of zirconia samples from different groups.

of TO_1, TO_2, and TO_3 samples was the rutile phase. Zirconia can transform from the tetragonal phase to the monoclinic phase in water or steam, especially under stress, which may cause microcracks and reduce material durability. This problem is most serious in dense zirconia that has been fully sintered, as it is more prone to low-temperature degradation (LTD).[23] In our study, the water bath treatment was applied to pre-sintered zirconia, so it does not cause LTD. Final high-temperature sintering both densifies the zirconia and restores the stable tetragonal phase. Thus, the risk of LTD in our process is very low. Titania typically crystallizes into the rutile phase after sintering at high temperatures (>800 °C). Previous studies have demonstrated that rutile, as a stable high-temperature phase, still possesses good biocompatibility and a certain degree of bioactivity, which can meet actual clinical requirements.[24] However, some studies reported that the anatase phase of TiO_2 generally exhibits superior bioactivity compared to the rutile phase.[25] In subsequent research, we will attempt to introduce other oxides to achieve the synthesis of a more bioactive anatase-phase TiO_2 coating. According to research, oxides can be an effective means of regulating the phase transformation of TiO_2: composite metal oxides can either promote or inhibit phase transitions.[26,27]

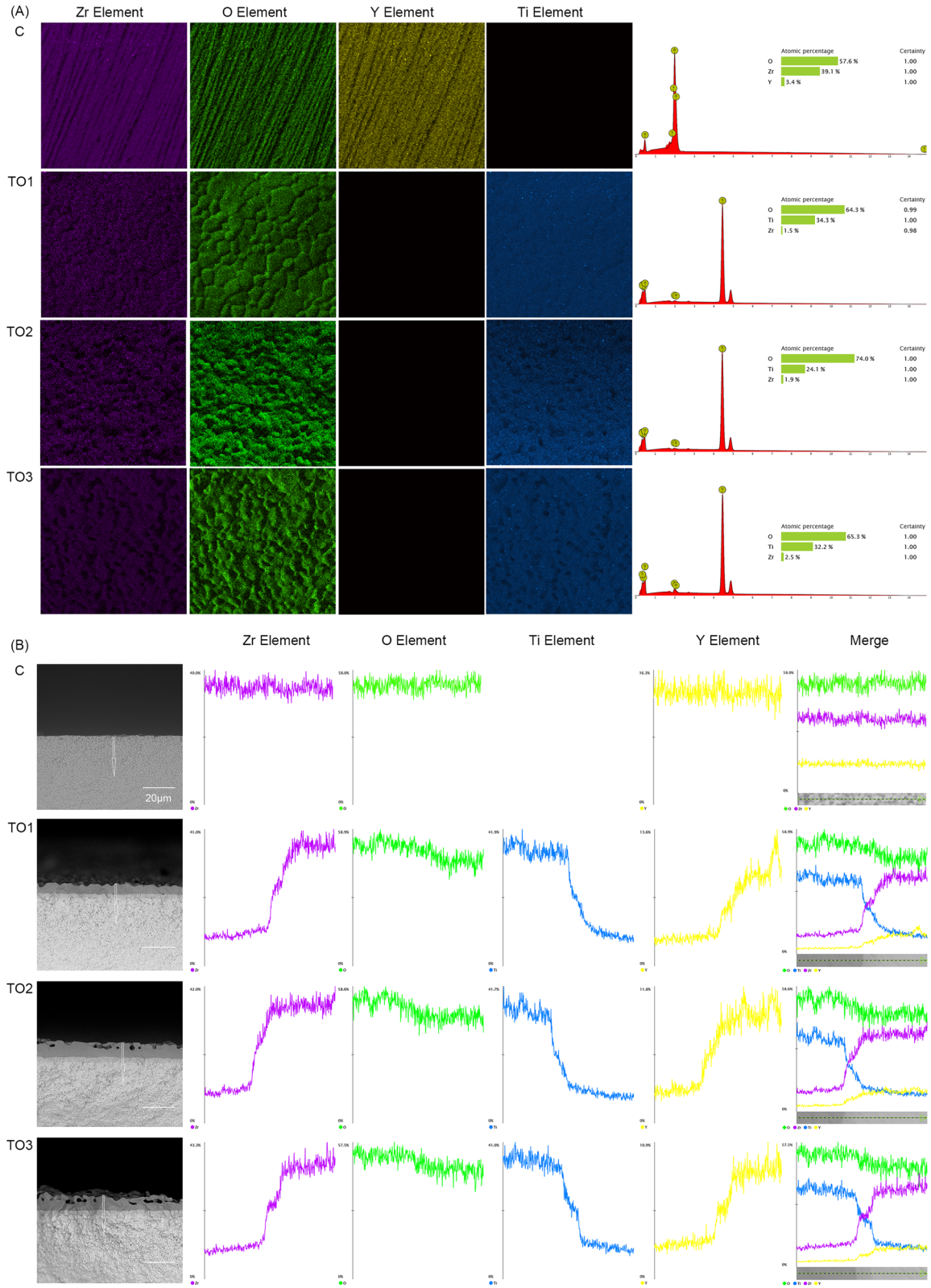

Fig. 2 (A) Elemental mapping of zirconia specimen surfaces in each group. (B) The EDS line-scanning results of longitudinal sections of zirconia.

The water contact angle measurements are presented in Fig. 3B and C. The titania coating significantly reduced the hydrophilicity of zirconia. The water contact angles of TO_2 and TO_3 groups were significantly lower than that of TO_1 ($p < 0.05$), while the TO_3 group exhibited the lowest value ($p < 0.05$). The enhanced hydrophilicity of porous titania coatings can be

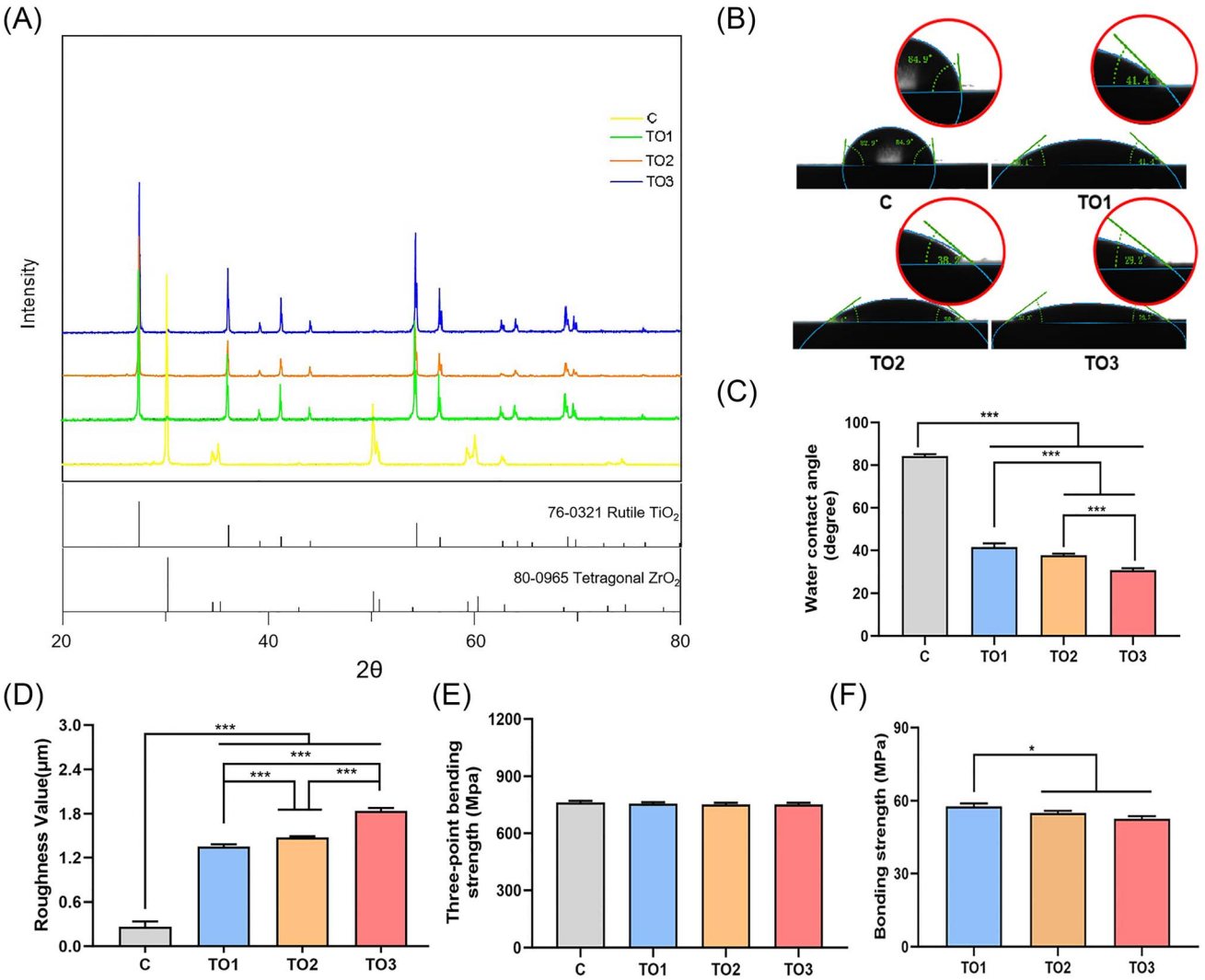

Fig. 3 (A) XRD patterns of diffrernt samples. (B and C) Water contact angles of each group zirconia. (D) Surface roughness value of the C, TO_1, TO_2, and TO_3 groups. (E) Three-point bending strength of the specimens. (F) Bonding strength of coatings from each group of samples. *P < 0.05, **P < 0.01, ***P < 0.001.

attributed to two factors. Firstly, TiO_2's highly polar Ti–O bonds promote water dissociation into hydroxyl groups, enhancing hydrophilicity.[28] Additionally, water contact angle decreases with increasing surface roughness.[29] The porous coating further improves hydrophilicity by enhancing surface roughness.

The surface roughness measurement results of zirconia specimens in each group are shown in Fig. 3D. The results indicated that the surface roughness of the control group was 0.26 ± 0.07 μm, while those of the TO_1, TO_2, and TO_3 groups were 1.35 ± 0.03 μm, 1.47 ± 0.02 μm and 1.84 ± 0.04 μm, respectively. The surface roughness values of the experimental groups were significantly higher than those of the control group (P < 0.001), and the TO_3 group exhibited significantly greater roughness compared to the other experimental groups (P < 0.001).

The flexural strength values of zirconia specimens in each group are shown in Fig. 3E. Compared with the group C, the zirconia specimens in groups TO_1, TO_2, and TO_3 exhibited reduced three-point bending strength. However, the differences among the groups were not statistically significant (P > 0.05). Rezaei *et al.* created micro–nano hierarchical structures on the surface of zirconia specimens using solid-state laser etching.[30] Their results showed that these structures significantly enhanced osseointegration. Additionally, Wang *et al.* prepared porous zirconia specimens *via* SLA-based 3D printing of zirconia slurry.[31] By fabricating porous morphological coatings on the surface of zirconia implants, they effectively improved the bioactivity of zirconia. Nevertheless, ensuring the mechanical strength of modified ceramic materials still requires extensive exploration. In this study, the results indicated that while hydrolysis of $ZrOCl_2$ produces acidic byproducts, which could theoretically weaken the zirconia substrate, the controlled concentration of $ZrOCl_2$ in this study did not compromise its mechanical strength. Moreover, unlike previous modification methods, the porous structure was introduced only in the

surface coating layer, preserving the dense core structure to maintain mechanical strength.

As shown in Fig. 3F, the bonding strengths of the coatings in the TO_1, TO_2, and TO_3 groups were 57.13 ± 0.84 MPa, 56.99 ± 0.81 MPa and 56.04 ± 0.22 MPa, respectively. There were no statistically significant differences between the TO_2 and TO_3 groups, but both were significantly lower than the group TO_1 ($P < 0.05$). Notably, the measured values in all groups met the 15 MPa requirement. Sini Rivari *et al.* prepared a titania coating on zirconia *via* the sol–gel method, enhancing epithelial cell adhesion, adhesion molecule expression, and cell diffusion on zirconia surfaces *in vitro*.[32] Additionally, Li Nan *et al.* fabricated a TiO_2 coating on zirconia by atomic layer deposition (ALD) technology, demonstrating that the titania coating significantly enhanced the osteogenic differentiation capacity of osteoblasts *in vitro* and *in vivo*.[33] However, the TiO_2 coatings obtained through these methods struggled to form a continuous and uniform layer on zirconia, and their bonding strength could not be guaranteed. In this study, the Ti–Zr transition layer was generated at the coating/substrate interface through hydrolysis-sintering process. This approach avoided stress concentration caused by thermal expansion coefficient mismatch, which is the primary reason for the delamination of traditional sprayed coatings. In our previous research, it was confirmed that the Ti–Zr mixed layer primarily consisted of a solid solution ($ZrTiO_4$), further enhancing interfacial stability.[19,34]

3.2. Cell survival and proliferation

The live/dead fluorescence staining was conducted to assess the cytotoxicity of different implants after 1 and 3 days of culture. Green fluorescence indicated live cells, while red fluorescence represented dead cells (Fig. 4A). The majority of cells adherent to the ZrO_2 discs in all groups remained viable (green), with a small number of dead cells (red). Therefore, it can be concluded that the porous titania coating exhibited good cytocompatibility.

The proliferation activity of MC3T3-E1 cells on different specimens is shown in Fig. 4B. After 1, 3, and 5 days of culture, the TO_1, TO_2, and TO_3 groups demonstrated significantly higher cell proliferation activity compared to the group C ($P < 0.05$). Among them, the porous TiO_2 coatings (TO_2 and TO_3) further enhanced proliferation compared to TO_1, with TO_3 exhibiting the highest activity ($P < 0.05$).

As shown in Fig. 4C, morphological analysis of MC3T3-E1 cells on the porous TiO_2 coating surface demonstrated that this porous structure significantly enhances cell adhesion and spreading.

Studies have demonstrated that the micro-scale surface roughness of implants plays a crucial role in osseointegration.[35] Compared to smooth surfaces, Wennerberg *et al.* found that surfaces with a roughness of 1–2 μm significantly enhance osteoblast proliferation and adhesion.[36] The surface topography of implants influences osteoblast adhesion behavior, primarily through the anchoring effect of actin-based cytoskeletal fibers in osteoblasts, which interact with the rough surface to promote cell-implant binding and facilitate early-stage cell adhesion.[37] Furthermore, porous structures facilitate cell adhesion and growth by providing mechanical interlocking during initial cell attachment, which is critical for enhancing osteoblast proliferation.[38] In this study, surface modification of zirconia not only enhanced surface roughness but also formed a porous titania coating, which significantly improved the substrate's suitability for cell adhesion and proliferation. The porous titania coating preparation method used in this study offers advantages such as simplicity of operation, controllable cost, and the ability to coat large areas, making it well-suited for clinical application and industrial promotion. The resulting porous structure effectively enhances surface roughness and specific surface area, thereby improving the environment for cell adhesion and providing an innovative pathway for the functionalization of implant surfaces. However, this method has certain limitations in terms of pore structure uniformity and tunability.

To achieve more precise control over the porosity and pore structure of ceramic implants, several common strategies are used. One is the template method, which employs organic or inorganic templates to introduce highly uniform and size-controllable pores into ceramic matrices.[39,40] Another approach is 3D printing technology. This method uses digital design to accurately control pore size, porosity, and structural distribution, enabling the fabrication of personalized bone implants.[41,42] While the template method allows for precise customization of porous structures, it suffers from complex processes, high costs, and challenges in mass production.[43,44] 3D printing excels in structural complexity and individualization, but is limited by its cost, precision, efficiency, and post-processing requirements.[45,46] Therefore, the application and promotion of these methods need to balance practical needs, costs, and technical challenges. In our future research, we will actively explore the integration of these methods with our current approach to further enhance the biological performance of the porous coatings.

Hydrophilicity is a critical parameter for evaluating the surface properties of biomaterials, as it directly influences their interactions with biological systems, particularly in cell adhesion, proliferation, and migration.[47] Studies have shown that materials with good surface hydrophilicity are more conducive to the early adhesion and spreading of osteoblasts, and the underlying mechanism may be related to increased expression of focal adhesion proteins and actin.[48,49] Hydrophilic surfaces offer distinct advantages by more effectively mimicking the natural cellular growth environment, thereby providing an optimal interface for cell development. After porous coating modification, the surface wettability of zirconia samples was significantly enhanced, promoting cell attachment and spreading, stimulating cell proliferation and osteogenic differentiation, and accelerating bone regeneration and osseointegration. As demonstrated by the morphological analysis of MC3T3-E1 cells seeded on the surfaces of zirconia specimens in this study, the TO_3 group, which had the lowest contact angle, exhibited the best osteoblast affinity. In contrast, the control group with a higher surface contact angle showed certain adverse effects on cell adhesion, spreading, and the formation of the actin cytoskeleton. The actin cytoskeleton is an

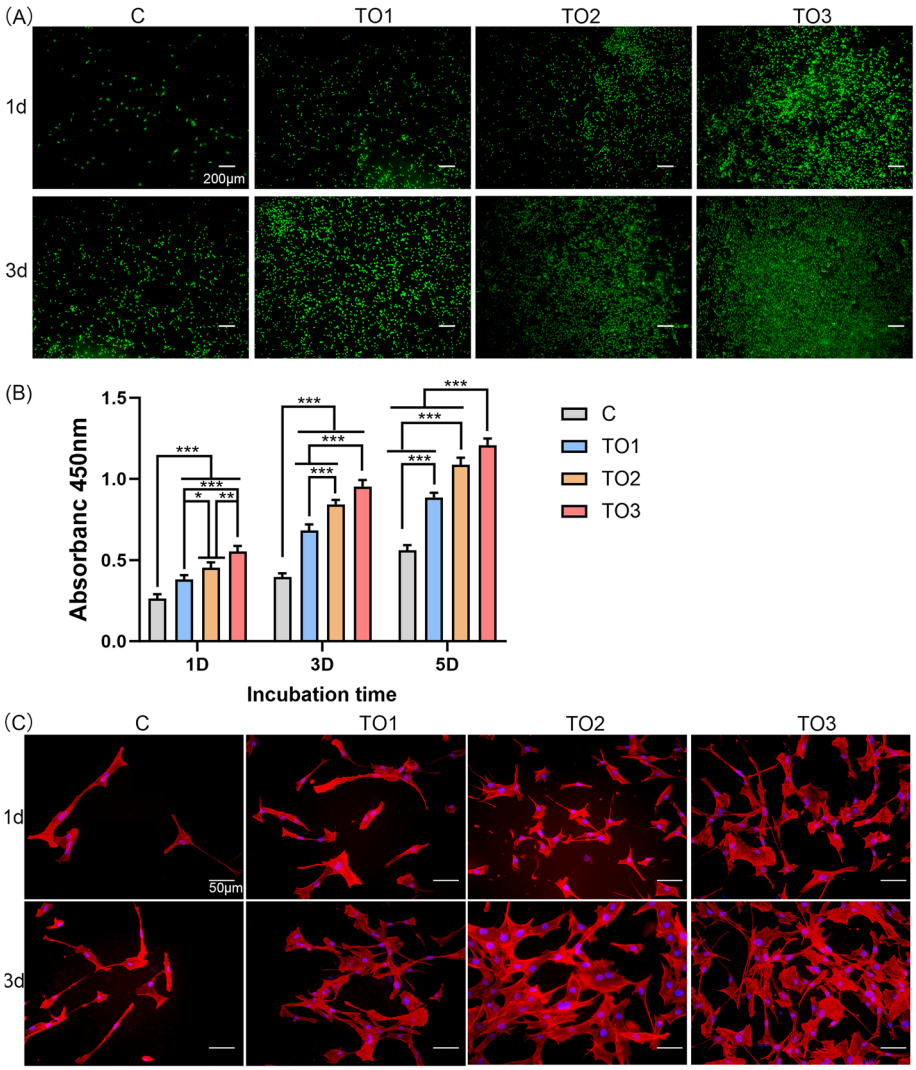

Fig. 4 (A) The live/dead fluorescence double staining of MC3T3-E1 cells cultured on different group samples for 1 and 3 days. (B) Proliferation of MC3T3-E1 cells seeded on each group of zirconia discs after 1, 3 and 5 days. (C) Cytoskeletal morphology of MC3T3-E1 cells incubated on different specimens for 1 and 3 days. *P < 0.05, **P < 0.01, ***P < 0.001.

important structure through which integrin proteins transmit forces between the interior and exterior of the cell. Studies have shown that hydrophobic surfaces reduce protein adsorption, and insufficient wettability can affect the initial interaction between the material surface and blood components as well as subsequent cellular responses.[50] As a result, improved surface hydrophilicity facilitates thorough wetting of biomaterials, which enhances the adsorption of bioactive molecules and supports osteoblast attachment, ultimately contributing to greater proliferation, differentiation, and mineralization of these cells.

Enhanced surface roughness and improved hydrophilicity are generally beneficial for promoting cell adhesion and osteogenic differentiation. In addition, the chemical characteristics of material surfaces play a crucial role in influencing cell behavior. For example, TiO_2 surfaces that are rich in Ti–OH groups are beneficial for protein adsorption and cell recruitment.[16] Furthermore, variations in TiO_2 crystal phases, such as rutile and anatase, can lead to differences in bioactivity.[51,52] In this study, the observed enhancement in cellular response can be attributed to the combined effects of these two factors.

3.3. *In vitro* osteogenic differentiation of porous TiO_2 coating

As shown in Fig. 5A, the ALP activity of MC3T3-E1 cells cultured on TiO_2-coated zirconia was significantly higher than that on zirconia substrates after 4 and 7 days of culture (P < 0.05). Notably, the porous TiO_2 coating (TO_2 and TO_3 groups) exhibited further enhanced ALP activity compared to the TO_1 group, with the TO_3 group demonstrating the highest ALP activity (P < 0.05).

Furthermore, Alizarin Red S (ARS) staining was performed to evaluate the osteogenic differentiation of cells seeded on different samples (Fig. 5B). The TO_3 group showed a significantly greater number of calcium nodules than the other

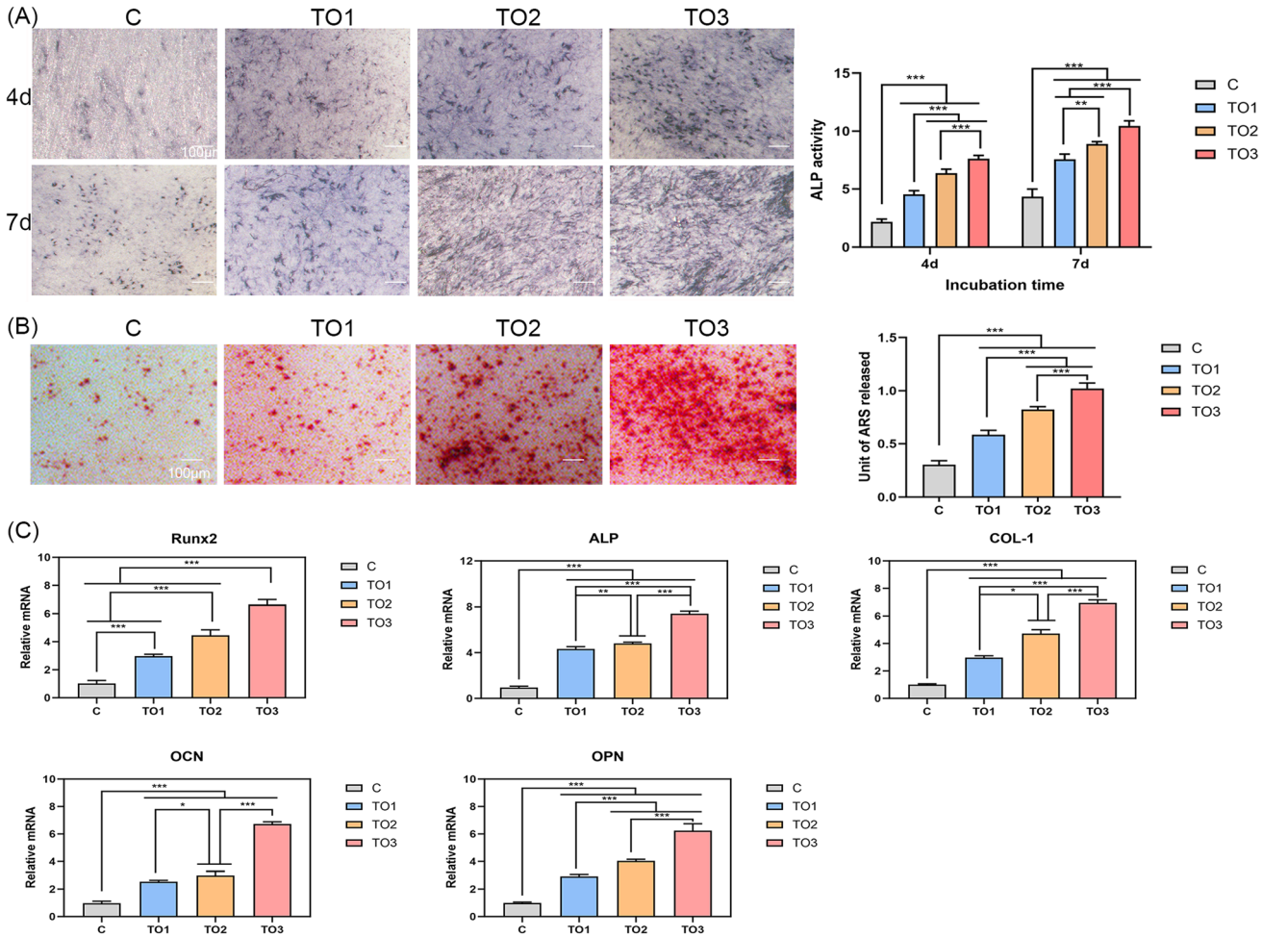

Fig. 5 (A) ALP stainingd and quantitative results of MC3T3-E1 cells seeded on different samples for 4 and 7 days. (B) ARS staining and quantitative results of MC3T3-E1 cells cultured on different specimens for 14 days. (C) The results of RT-qPCR analysis of osteogenic differentiation-related genes in MC3T3-E1 cells co-cultured with C, TO_1, TO_2 and TO_3 groups for 7 days. *$P < 0.05$, **$P < 0.01$, ***$P < 0.001$.

groups, indicating enhanced extracellular matrix mineralization. Quantitative analysis of ARS staining confirmed that the porous TiO_2-modified zirconia surface significantly promoted osteogenic differentiation of MC3T3-E1 cells compared to other groups ($P < 0.05$).

After 7 days of co-culture, the TO_3 group exhibited significantly upregulated expression of osteogenic-related genes (Runx2, ALP, COl-1, OCN and OPN) compared to the TO_1 and TO_2 groups ($P < 0.05$). Moreover, all experimental groups showed significantly higher expression than the C group (Fig. 5C). In conclusion, the porous TiO_2 coating significantly enhances the osteointegration capacity of cells.

ALP is an enzyme secreted during osteoprogenitor cell differentiation and is recognized as an early biomarker of bone formation.[53] ALP activity directly reflects the osteogenic potential of cells. Alizarin Red can chelate calcium salts deposited by cells, forming mineralized nodules.[54] Late-stage mineralization of cells cultured on zirconia specimens was evaluated quantitatively through Alizarin Red staining. The osteogenic gene expression of cells seeded on the surface of zirconia samples from each group was evaluated through qRT-PCR. ALP serves as an early-stage osteogenic marker, while OCN and OPN are two critical proteins involve in late-stage osteost mineralization. Runx2 is a specific transcription factor in osteogenic differentiation. CoL-I is not only a vital organic component of bone tissue but also a key marker protein for mature osteogenic differentiation.[55,56]

In this study, the titania coating of the TO1 group significantly enhanced the osteogenic differentiation of surface-seeded cells compared to the group C. However, the surface morphology of the TO_1 was relatively uniform and lacked a porous structure, failing to provide sufficient attachment sites and growth space for cells, thereby limiting their migration, proliferation, and differentiation capabilities. Moreover, the coating's bioactivity holds further potential for enhancement. A porous morphology could increase the specific surface area, further promoting protein adsorption and *in vitro* mineralization. Consequently, the co-cultured cells in the TO_2 and TO_3 groups exhibited superior differentiation effects compared to TO_1, with the TO_3 group demonstrating the best performance.

The porous structure significantly increases the specific surface area of the material, providing favorable space for bone

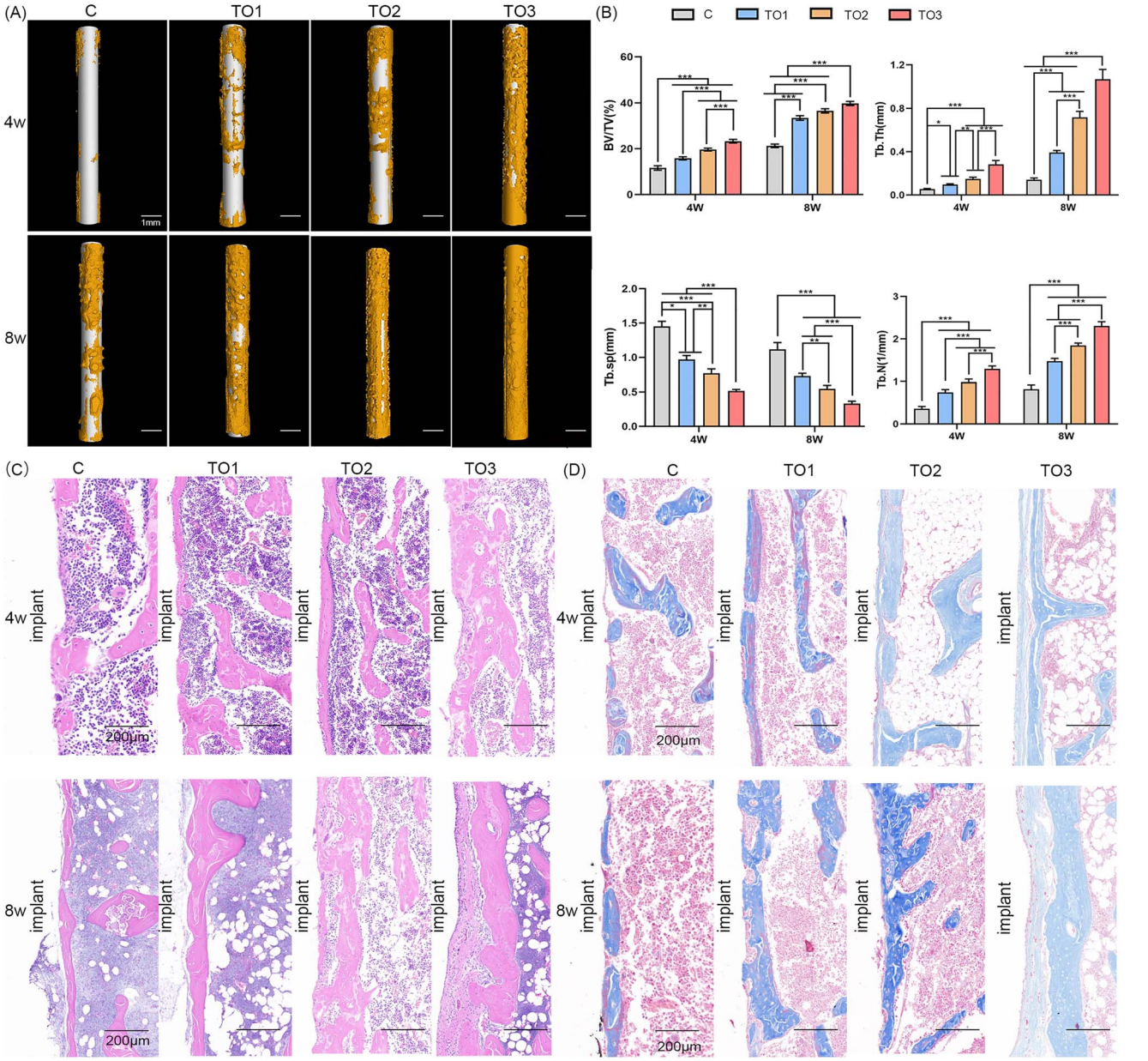

Fig. 6 (A) Representative 3D micro-CT reconstructions of peri-implant bone at 4 and 8 w. (B) Quantitative analyses of BV/TV, Tb. Th, Tb. Sp and Tb. N according to the micro-CT scanning. (C) H&E and (D) Masson's Trichrome stating of the new bone formation around the implant at 4 and 8 weeks. *P < 0.05, **P < 0.01, ***P < 0.001.

ingrowth and osseointegration. Porous materials with interconnected and appropriately sized pores not only facilitate cell adhesion, but also promote nutrient distribution through neovascularization and enhance osteogenic capacity.[57–59] Studies have found that the implantation of porous materials can upregulate fibrinogen to form a fibrin network, which supports cell attachment and migration, promotes collagen synthesis and angiogenesis, and reduces the pro-inflammatory response of macrophages, thereby inducing them to promote the osteogenic differentiation of mesenchymal stem cells.[60,61] In addition, porous materials can modulate signaling pathways such as NF-κB, focal adhesions, cytoskeletal tension, and integrin-FAK-ERK1/2, thereby influencing the activity of key transcription factors like YAP and RUNX2, and regulating the self-renewal and osteogenic differentiation of mesenchymal stem cells.[62,63] Microarray bioinformatics studies have also shown that the β-catenin pathway plays a key role in mediating osteogenic differentiation on porous TiO_2 surfaces.[64] In summary, porous TiO_2 coatings enhance osseointegration by optimizing the surface structure and chemical properties of zirconia implants, thus improving the adhesion, proliferation, and differentiation of osteogenic cells. Nevertheless, further systematic studies are needed in the future to elucidate the relevant signaling networks and their regulatory mechanisms.

3.4. *In vivo* osseointegration assessment

The Micro-CT analysis (Fig. 6A) showed that at 4 weeks post-implantation, group C exhibited larger bone defects around the implants, while the titania-coated group had smaller defects with enhanced osteogenesis. The TO_3 group showed superior osteogenic performance to TO_1 and TO_2 groups. By 8 weeks, new bone formation was observed in all groups, with TO_3 achieving complete defect regeneration through uniform bone formation.

Fig. 6B presents the statistical results of bone tissue around the implants in each group at 4 and 8 weeks post-implantation. The TO_3 group exhibited the highest levels of bone volume fraction (BV/TV), trabecular thickness (Tb. Th), and trabecular number (Tb. N), along with the smallest trabecular separation (Tb. Sp) in the newly formed bone around the implants ($P < 0.05$). Additionally, the TO_2 group demonstrated superior bone-related parameters compared to the TO_1 group ($P < 0.05$), while group C showed the least favorable outcomes ($P < 0.05$).

The formation of new bone tissue and implant-bone contact in the femur with implants were evaluated through H&E and Masson staining. As shown in Fig. 6C and D, only minimal new bone formation was observed between the implant and native bone in group C. In contrast, the titania-coated zirconia implants demonstrated significantly enhanced osteogenic activity. Moreover, the TO_3 group exhibited substantial new bone formation, with the bone defect area at the implant edges connected to fibrous connective tissue, indicating successful osseointegration and continued bone growth.

The formation of osseointegration between implants and surrounding bone tissue involves complex physiological reactions. *In vivo* animal experiments were conducted to comprehensively evaluate the effect of porous titania-coated zirconia on osseointegration. Bone volume fraction (BV/TV) is a widely used parametera for assessing bone mass, directly reflecting changes in bone volume. Trabecular bone is a three-dimensional network structure, with trabecular thickness (Tb. Th), trabecular number (Tb. N), and trabecular separation (Tb. Sp) serving as key indicators for evaluating its spatial architecture.[65,66]

The surface characteristics of implants, including chemical composition and morphological structure, significantly influence their post-implantation repair outcomes. These factors play a crucial role in determining the osseointegration capability of implants.[67] In this study, a porous titania coating was applied to the surface of zirconia implants, which not only increased surface roughness and wettability but also introduced a porous microstructure, thereby enhancing the osseointegration capacity of the implants.

4. Conclusion

The porous TiO_2 coatings on zirconia implants effectively optimized surface topography and wettability. These modified surfaces significantly enhanced MC3T3-E1 cells proliferation, spreading, mineralization, and osteogenic gene expression. *In vivo* studies further demonstrated superior bone ingrowth and enhanced trabecular remodeling with the porous TiO_2-coated implants. These findings highlight the clinical potential of porous TiO_2 surface modification in enhancing osseointegration and expanding the applications of zirconia implants.

Conflicts of interest

The authors declare that the research was conducted in the absence of any commercial or financial relationships that could be construed as a potential conflict of interest.

Data availability

All data underlying the results are available as part of the article and no additional source data is required.

Acknowledgements

This work was supported by the Beijing Stomatological Hospital, Capital Medical University Young Scientist Program (No. YSP202318).

References

1 M. Ciszyński, B. Chwaliszewski, W. Simka, M. Dominiak, T. Gedrange and J. Hadzik, Zirconia Dental Implant Designs and Surface Modifications: A Narrative Review, *Materials*, 2024, **17**, 4202.
2 B. Chen, W. Wang, M. Hu, Y. Liang, N. Wang, C. Li and Y. Li, "Photo-Thermo-Electric" Dental Implant for Anti-Infection and Enhanced Osteoimmunomodulation, *ACS Nano*, 2024, **10**, 24968–24983.
3 N. M. Padhye, E. Calciolari, A. N. Zuercher, S. Tagliaferri and N. Donos, Survival and success of zirconia compared with titanium implants: a systematic review and meta-analysis, *Clin. Oral Invest.*, 2023, **27**, 6279–6290.
4 M. K. Thu, Y. S. Kang, J. M. Kwak, Y. H. Jo, J. S. Han and I. L. Yeo, Comparison between bone-implant interfaces of microtopographically modified zirconia and titanium implants, *Sci. Rep.*, 2023, **13**, 11142.
5 C. Gautam, J. Joyner, A. Gautam, J. Rao and R. Vajtai, Zirconia based dental ceramics: structure, mechanical properties, biocompatibility and applications, *Dalton Trans.*, 2016, **45**, 19194–19215.
6 B. Arefnia, O. Fakheran, N. Jakse and M. Payer, Patient-reported outcomes of zirconia dental implants: a systematic review and future directions, *J. Patient-Rep. Outcomes*, 2025, **9**, 7.
7 F. H. Schunemann, M. E. Galarraga-Vinueza, R. Magini, M. Fredel, F. Silva, J. Souza, Y. Zhang and B. Henriques, Zirconia surface modifications for implant dentistry, *Mater. Sci. Eng., C*, 2019, **98**, 1294–1305.
8 J. Chile, A. Dolores, F. Espinoza-Carhuancho, D. Alvitez-Temoche, A. Munive-Degregori, J. Barja-Ore and F. Mayta-Tovalino, Zirconia Dental Implants as a Different Alternative to Titanium: A Literature Review, *J. Int. Soc. Prev. Community Dent.*, 2023, **13**, 357–364.

9 S. J. Sadowsky, Has zirconia made a material difference in implant prosthodontics? A review, *Dent. Mater.*, 2020, **36**, 1–8.
10 A. Hafezeqoran and R. Koodaryan, Effect of Zirconia Dental Implant Surfaces on Bone Integration: A Systematic Review and Meta-Analysis, *BioMed Res. Int.*, 2017, **2017**, 9246721.
11 J. Fischer, A. Schott and S. Martin, Surface micro-structuring of zirconia dental implants, *Clin. Oral Implants Res.*, 2016, **27**(2), 162–166.
12 H. Xie, S. Shen, M. Qian, F. Zhang, C. Chen and F. R. Tay, Effects of Acid Treatment on Dental Zirconia: An In Vitro Study, *PLoS One*, 2015, **10**, e136263.
13 I. L. Aurelio, A. M. Marchionatti, A. F. Montagner, L. G. May and F. Z. Soares, Does air particle abrasion affect the flexural strength and phase transformation of Y-TZP? A systematic review and meta-analysis, *Dent. Mater.*, 2016, **32**, 827–845.
14 M. Stefanic, K. Krnel and T. Kosmac, Novel method for the synthesis of a β-tricalcium phosphate coating on a zirconia implant, *J. Eur. Ceram. Soc.*, 2013, **33**, 3455–3465.
15 X. Miao, Y. Hu, J. Liu and X. Huang, Hydroxyapatite coating on porous zirconia, *Mater. Sci. Eng., C*, 2007, **27**, 257–261.
16 Y. Hong, M. Yu, J. Lin, K. Cheng, W. Weng and H. Wang, Surface hydroxyl groups direct cellular response on amorphous and anatase TiO_2 nanodots, *Colloids Surf., B*, 2014, **123**, 68–74.
17 R. Miranda, W. J. Miranda, D. Lazar, V. Ussui, J. Marchi and P. F. Cesar, Effect of titania content and biomimetic coating on the mechanical properties of the Y-TZP/TiO_2 composite, *Dent. Mater.*, 2018, **34**, 238–245.
18 J. Si, J. Zhang, S. Liu, W. Zhang, D. Yu, X. Wang, L. Guo and S. G. Shen, Characterization of a micro-roughened TiO_2/ZrO_2 coating: mechanical properties and HBMSC responses in vitro, *Acta Biochim. Biophys. Sin.*, 2014, **46**, 572–581.
19 S. Tang, J. Zhang, N. Ding and Z. Zhang, Biological activity of titania coating prepared with zirconium oxychloride and titania on zirconia surface, *J. Mech. Behav. Biomed. Mater.*, 2021, **123**, 104780.
20 Q. Ma, Q. Ding, L. Zhang, Y. Sun and Q. Xie, Surface Characteristics and Flexural Strength of Porous-Surface Designed Zirconia Manufactured via Stereolithography, *J. Prosthodont.*, 2023, **2**, e81–e89.
21 T. T. Dele-Afolabi, M. A. A. Hanim, M. Norkhairunnisa, S. Sobri and R. Calin, Research trend in the development of macroporous ceramic components by pore forming additives from natural organic matters: a short review, *Ceram. Int.*, 2017, **43**, 1633–1649.
22 C. Hadjicharalambous, E. Mygdali, O. Prymak, A. Buyakov, S. Kulkov and M. Chatzinikolaidou, Proliferation and osteogenic response of MC3T3-E1 pre-osteoblastic cells on porous zirconia ceramics stabilized with magnesia or yttria, *J. Biomed. Mater. Res., Part A*, 2015, **103**, 3612–3624.
23 K. A. Al-Aali, S. Alresayes, A. M. Alhenaki, F. Vohra and T. Abduljabbar, Influence of time and hydration (ageing) on flexural strength of Yttrium stabilized Zirconia polycrystals (Y-TZP) fabricated with different CAD-CAM Systems, *J. Med. Sci.*, 2021, **37**, 833–839.
24 Y. Bai, I. S. Park, H. H. Park, M. H. Lee, T. S. Bae, W. Duncan and M. Swain, The effect of annealing temperatures on surface properties, hydroxyapatite growth and cell behaviors of TiO_2 nanotubes, *Surf. Interface Anal.*, 2011, **43**, 6.
25 K. K. Ghose, Y. Liu and T. J. Frankcombe, Comparative first-principles structural and vibrational properties of rutile and anatase TiO_2, *J. Phys. Condens. Matter*, 2023, **21**, 35.
26 J. C. Colmenares, M. A. Aramendía, A. Marinas, J. M. Marinas and F. J. Urbano, Synthesis, characterization and photocatalytic activity of different metal-doped titania systems, *Appl. Catal., A*, 2006, **306**, 120–127.
27 J. P. Xu, S. B. Shi, L. Li, J. F. Wang, L. Y. Lv, F. M. Zhang and Y. W. Du, Effect of manganese ions concentration on the anatase-rutile phase transformation of TiO_2 films, *J. Phys. Chem. Solid.*, 2009, **70**(3–4), 511–515.
28 Y. Hong, M. Yu, J. Lin, K. Cheng, W. Weng and H. Wang, Surface hydroxyl groups direct cellular response on amorphous and anatase TiO_2 nanodots, *Colloids Surf., B*, 2014, **123**, 68–74.
29 F. Rupp, L. Scheideler, N. Olshanska, M. de Wild, M. Wieland and J. Geis-Gerstorfer, Enhancing surface free energy and hydrophilicity through chemical modification of microstructured titanium implant surfaces, *J. Biomed. Mater. Res., Part A*, 2006, **76**, 323–334.
30 N. M. Rezaei, M. Hasegawa, M. Ishijima, K. Nakhaei, T. Okubo, T. Taniyama, A. Ghassemi, T. Tahsili, W. Park, M. Hirota and T. Ogawa, Biological and osseointegration capabilities of hierarchically (meso-/micro-/nano-scale) roughened zirconia, *Int. J. Nanomed.*, 2018, **13**, 3381–3395.
31 Z. Wang, Q. Ding, Y. Gao, Q. Q. Ma, L. Zhang, X. Y. Ge, Y. C. Sun and Q. F. Xie, Effect of porous zirconia ceramics on proliferation and differentiation of osteoblasts, *Beijing Daxue Xuebao, Yixueban*, 2022, **54**, 31–39.
32 S. Riivari, E. Närvä, I. Kangasniemi, J. Willberg and T. Närhi, Epithelial cell attachment and adhesion protein expression on novel in sol TiO_2 coated zirconia and titanium alloy surfaces, *J. Biomed. Mater. Res., Part B*, 2022, **110**, 2533–2541.
33 N. Li, Z. Liu, G. Liu, Z. Wang, X. Guo, C. Guo and J. Han, TiO_2 Nanocoatings with Controllable Crystal Type and Nanoscale Topography on Zirconia Implants to Accelerate Bone Formation, *Bioinorg. Chem. Appl.*, 2022, **2022**, 8650659.
34 K. Bahranowski, A. Klimek, A. Gaweł, K. Górniak, A. Michalik and E. Serwicka-Bahranowska, Structural Transformations of Hydrolysates Obtained from Ti-, Zr-, and Ti, Zr-Solutions Used for Clay Pillaring: Towards Understanding of the Mixed Pillars Nature, *Materials*, 2018, **24**, 44.
35 J. Lincks, B. D. Boyan, C. R. Blanchard, C. H. Lohmann, Y. Liu, D. L. Cochran, D. D. Dean and Z. Schwartz, Response of MG63 osteoblast-like cells to titanium and titanium alloy is dependent on surface roughness and composition, *Biomaterials*, 1998, **19**, 2219–2232.
36 A. Wennerberg and T. Albrektsson, Effects of titanium surface topography on bone integration: a systematic review, *Clin. Oral Implants Res.*, 2009, **20**, 172–184.
37 T. Miyauchi, M. Yamada, A. Yamamoto, F. Iwasa, T. Suzawa, R. Kamijo, K. Baba and T. Ogawa, The enhanced

characteristics of osteoblast adhesion to photofunctionalized nanoscale TiO_2 layers on biomaterials surfaces, *Biomaterials*, 2010, **31**, 3827–3839.
38 X. Wang, K. Zhou, Y. Li, H. Xie and B. Wang, Preparation, modification, and clinical application of porous tantalum scaffolds, *Front. Bioeng. Biotechnol.*, 2023, **11**, 1127939.
39 J. H. Ku, S. C. Ho, H. A. Myung, Y. K. Ji and H. Soo, Tuning the porosity of TiO_2 nanoparticles via surfactant-templated aerosol process for enhanced photocatalytic reactivity, *Chem. Phys. Lett.*, 2019, **715**, 134–140.
40 H. Choi, Y. J. Kim, R. S. Varma and D. D. Dionysiou, Thermally Stable Nanocrystalline TiO_2 Photocatalysts Synthesized via Sol–Gel Methods Modified with Ionic Liquid and Surfactant Molecules, *Chem. Mater.*, 2015, **18**, 22.
41 Y. Zheng, Q. Han, J. Wang, D. Li, Z. Song and J. Yu, Promotion of Osseointegration between Implant and Bone Interface by Titanium Alloy Porous Scaffolds Prepared by 3D Printing, *ACS Biomater. Sci. Eng.*, 2020, **14**(6), 5181–5190.
42 Z. Yi, Y. Liu, Y. D. Ma, Z. Liu, H. Sun, X. Zhou, R. Kang, V. A. M. Cristino and Q. Wang, Surface treatment of 3D printed Cu-bearing Ti alloy scaffolds for application in tissue engineering, *Mater. Des.*, 2022, **213**, 110350.
43 N. Hedayat, Y. Du and H. Ilkhani, Review on fabrication techniques for porous electrodes of solid oxide fuel cells by sacrificial template methods, *Renewable Sustainable Energy Rev.*, 2017, **77**, 1221–1239.
44 K. Schelm, E. Abreu Morales and M. Scheffler, Mechanical and Surface-Chemical Properties of Polymer Derived Ceramic Replica Foams, *Materials*, 2019, **12**, 1870.
45 H. Xie, X. Yang, P. Liu, X. Xu, Z. Zhou, W. Zhao and Z. Shen, 3D gel printing of alumina ceramics followed by efficient multi-step liquid desiccant drying, *J. Eur. Ceram. Soc.*, 2021, **41**, 6634–6640.
46 J. Deckers, S. Meyers, J. P. Kruth and J. Vleugels, Direct selective laser sintering/melting of high density alumina powder layers at elevated temperatures, *Phys. Procedia*, 2014, **56**, 117–124.
47 S. Anjum, D. K. Arya, M. Saeed, D. Ali, M. S. Athar, W. Yulin, S. Alarifi, X. Wu, P. S. Rajinikanth and Q. Ao, Multifunctional electrospun nanofibrous scaffold enriched with alendronate and hydroxyapatite for balancing osteogenic and osteoclast activity to promote bone regeneration, *Front. Bioeng. Biotechnol.*, 2023, **11**, 1302594.
48 T. G. van Kooten, H. T. Spijker and H. J. Busscher, Plasma-treated polystyrene surfaces: model surfaces for studying cell-biomaterial interactions, *Biomaterials*, 2004, **25**, 1735–1747.
49 Y. Han, D. Chen, J. Sun, Y. Zhang and K. Xu, UV-enhanced bioactivity and cell response of micro-arc oxidized titania coatings, *Acta Biomater.*, 2008, **4**, 1518–1529.
50 E. A. Voger and R. W. Bussian, Short-term cell-attachment rates: a surface-sensitive test of cell-substrate compatibility, *J. Biomed. Mater. Res.*, 1987, **21**, 1197–1211.
51 W. Q. Yu, Y. L. Zhang, X. Q. Jiang and F. Q. Zhang, In vitro behavior of MC3T3-E1 preosteoblast with different annealing temperature titania nanotubes, *Oral Dis.*, 2010, **16**, 624–630.
52 J. He, W. Zhou, X. Zhou, X. Zhong, X. Zhang, P. Wan, B. Zhu and W. Chen, The anatase phase of nanotopography titania plays an important role on osteoblast cell morphology and proliferation, *J. Mater. Sci. Mater. Med.*, 2008, **19**, 3465–3472.
53 R. Fraioli, K. Dashnyam, J. H. Kim, R. A. Perez, H. W. Kim, J. Gil, M. P. Ginebra, J. M. Manero and C. Mas-Moruno, Surface guidance of stem cell behavior: Chemically tailored co-presentation of integrin-binding peptides stimulates osteogenic differentiation in vitro and bone formation in vivo, *Acta Biomater.*, 2016, **43**, 269–281.
54 R. P. Ocaña, G. D. Rabelo, L. M. Sassi, V. P. Rodrigues and F. A. Alves, Implant osseointegration in irradiated bone: an experimental study, *J. Periodontal. Res.*, 2017, **52**, 505–511.
55 L. Chen, D. Wang, F. Peng, J. Qiu, L. Ouyang, Y. Qiao and X. Liu, Correction to Nanostructural Surfaces with Different Elastic Moduli Regulate the Immune Response by Stretching Macrophages, *Nano Lett.*, 2020, **20**, 2932–2933.
56 Y. Hu, K. Cai, Z. Luo, Y. Zhang, L. Li, M. Lai, Y. Hou, Y. Huang, J. Li, X. Ding, B. Zhang and K. L. Sung, Regulation of the differentiation of mesenchymal stem cells in vitro and osteogenesis in vivo by microenvironmental modification of titanium alloy surfaces, *Biomaterials*, 2012, **33**, 3515–3528.
57 H. D. Kim, S. Amirthalingam, S. L. Kim, S. S. Lee, J. Rangasamy and N. S. Hwang, Biomimetic materials and fabrication approaches for bone tissue engineering, *Adv. Healthcare Mater.*, 2017, **6**, 10.
58 Z. P. Cu, X. Zhang, L. Li, Q. G. Wang, X. X. Yu and T. Feng, Acceleration of segmental bone regeneration in a rabbit model by strontium-doped calcium polyphosphate scaffold through stimulating VEGF and bFGF secretion from osteoblasts, *Mater. Sci. Eng., C*, 2013, **33**, 274–281.
59 R. F. do Prado, S. B. Rabêlo, D. P. de Andrade, R. D. Nascimento, V. A. Henriques, Y. R. Carvalho, C. A. Cairo and L. M. de Vasconcellos, Porous titanium and Ti-35Nb alloy: effects on gene expression of osteoblastic cells derived from human alveolar bone, *J. Mater. Sci. Mater. Med.*, 2015, **26**, 259.
60 M. Bessa-Gonçalves, A. M. Silva, J. P. Brás, H. Helmholz, B. J. C. Luthringer-Feyerabend, R. Willumeit-Römer, M. A. Barbosa and S. G. Santos, Fibrinogen and magnesium combination biomaterials modulate macrophage phenotype, NF-kB signaling and crosstalk with mesenchymal stem/stromal cells, *Acta Biomater.*, 2020, **114**, 471–484.
61 M. Bessa-Gonçalves, C. Ribeiro-Machado, M. Costa, C. C. Ribeiro, J. N. Barbosa, M. A. Barbosa and S. G. Santos, Magnesium incorporation in fibrinogen scaffolds promotes macrophage polarization towards M2 phenotype, *Acta Biomater.*, 2023, **155**, 667–683.
62 K. S. Alharbi, O. Afzal, A. S. A. Altamimi, W. H. Almalki, I. Kazmi, F. A. Al-Abbasi, S. I. Alzarea, H. A. Makeen and M. Albratty, Potential role of nutraceuticals via targeting a Wnt/β-catenin and NF-κB pathway in treatment of osteoarthritis, *J. Food Biochem.*, 2022, **46**, 14427.
63 Y. U. Kuvyrkou, N. Brezhneva, E. V. Skorb and S. A. Ulasevich, The influence of the morphology of titania

and hydroxyapatite on the proliferation and osteogenic differentiation of human mesenchymal stem cells, *RSC Adv.*, 2021, **11**, 3843–3853.

64 W. Yu, Y. Zhang, L. Xu, S. Sun, X. Jiang and F. Zhang, Microarray-based bioinformatics analysis of osteoblasts on TiO_2 nanotube layers, *Colloids Surf., B*, 2012, **93**, 135–142.

65 A. M. Delany and K. D. Hankenson, Thrombospondin-2 and SPARC/osteonectin are critical regulators of bone remodeling, *J. Cell Commun. Signal.*, 2009, **3**, 227–238.

66 L. Ni, L. Zhang, W. Xia, G. Chen, X. Cui, W. Zhang, Z. Luo and H. Yang, Disc degeneration promotes regional inhomogeneity in the trabecular morphology of loaded rat tail vertebrae, *J. Orthop. Transl.*, 2018, **15**, 104–111.

67 B. B. Sarvaiya, S. Kumar, M. S. H. Pathan, S. Patel, V. Gupta and M. Haque, The Impact of Implant Surface Modifications on the Osseointegration Process: An Overview, *Cureus*, 2025, **17**, e81576.